Mostafa A. H. Abdelmohimen[1]
Department of Mechanical Engineering,
College of Engineering,
King Khalid University,
Abha 61421, Saudi Arabia;
Department of Mechanical Engineering,
Shoubra Faculty of Engineering,
Benha University,
Cairo 12356, Egypt
e-mail: mostafa.abdelmohimen@feng.bu.edu.eg

Salem Algarni
Department of Mechanical Engineering,
College of Engineering,
King Khalid University,
Abha 61421, Saudi Arabia
e-mail: saalgarni@kku.edu.sa

Khalid Almutairi
Department of Mechanical Engineering,
College of Engineering,
University of Hafr Al Batin,
Hafr Al Batin 53264, Saudi Arabia
e-mail: khalid.almutairi@uhb.edu.sa

Gulam M. S. Ahmed
Department of Mechanical Engineering,
College of Engineering,
King Khalid University,
Abha 61421, Saudi Arabia
e-mail: gmsa786@kku.edu.sa

Kashif Irshad
Center of Research Excellence in Renewable Energy (CoRE-RE),
King Fahd University of Petroleum & Minerals,
Dhahran 31261, Saudi Arabia
e-mail: kashif.irshad@kfupm.edu.sa

Sayed A. Irfan
Department of Fundamental and Applied Sciences,
Universiti Teknologi Petronas,
Bandar Seri Iskandar, Perak 32610, Malaysia
e-mail: sayed.irfan@utp.edu.my

Improving Heat Transfer of Plate-Fin Heat Sinks Using Through Rod Configurations

The performance of the heat sink has been investigated as using rods through its fins. The shear-stress transport k–ω model is selected to carry out this study. Two different flow directions have been studied. Four cases are represented, including the baseline case which has no rods through the fins. Two, four, and six rods are used through the fins. Thermal resistance, pumping power, and Nusselt number have been represented and discussed through this study. The results show that as the number of rods increases, the thermal resistance decreases while the required pumping power increases. The impinging flow direction shows higher performance as compared with the suction flow direction. As the Reynolds number increases, the Nusselt number increases for all studied cases. The optimum case along with the studied range of Reynolds number and number of rods is case-2 (has four rods through fins). [DOI: 10.1115/1.4046984]

Keywords: extended surfaces/fins, forced convection, heat transfer enhancement, thermal systems

1 Introduction

Many applications depend on heat sinks to loss or gain heat from a source. Electronics and microelectronic equipment are one of those application where increasing the heat transfer rate is critically essential for the long-term reliable operation. The design of heat sinks is affected by many factors such as the material conductivity, temperature range, air flow types (free of forced), and cost of production [1]. The thermal performance of the heat sink depends on its geometry. Increasing the contact area and the flow behavior through the heat sink attracts the researcher's attention long time ago. Plate and pin fins are assumed to be the best cost and manufacturing techniques available [1]. Plate-fin and pin-fin heat sinks are widely used in the industry due to simple design and easy fabrication [2]. Many studies have been focused on plate-fin heat sinks subject to an impinging flow [3–5]. Many studies have also focused on pin-fin heat sinks [6–10]. Comparison of the thermal performance of plate-fin and pin-fin heat sinks have been represented by many researchers [2,11–14]. Kim et al. [2] study experimentally and numerically the performance of both plate-fin and pin-fin heat sinks subject to an impinging flow. They showed that as the dimensionless length of heat sinks is small and the dimensionless pumping power is large, the optimized plate-fin heat sinks have smaller thermal resistances. Improving the performance of the plate-fin heat sinks also carried out with many researchers [15–18]. Wong and Indran [15] investigated numerically the heat transfer and fluid flow characteristics of a plate-fin heat sink subject to an impinging flow to describe the effect of fillet profiles at the bottom of the plate fin. Hussain et al. [16] investigated numerically the effect of flow direction and fillet profile on the heat transfer in plate-fin heat

[1]Corresponding author.

Manuscript received January 21, 2020; final manuscript received March 4, 2020; published online June 18, 2020. Assoc. Editor: Matthew Oehlschlaeger.

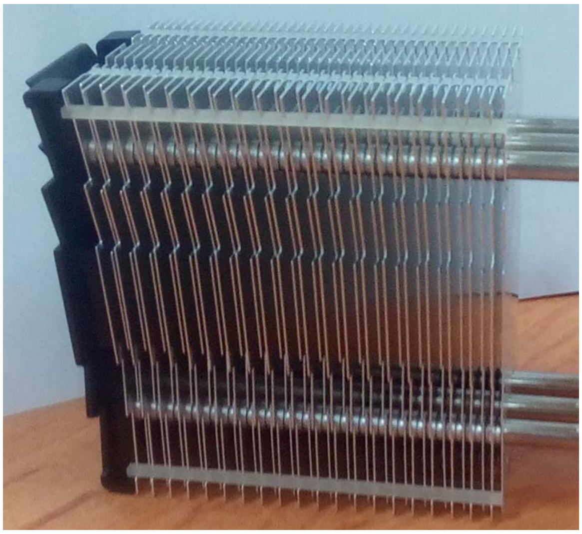

Fig. 1 Photo of a heat sink with through-fin rods

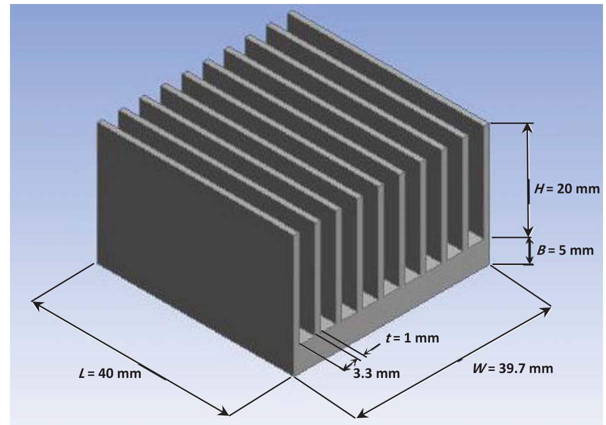

Fig. 2 Baseline case with dimensions

sinks. The results of this study show that the thermal resistance and base temperature reduce for the fillet profile. Jeon and Byon [17] investigate the performance of plate-fin heat sinks with dual-height fins subject to natural convection. Their results show that as the secondary fin height decreases, the thermal performance of the dual-height heat sink monotonically decreases for a fixed value of the primary fin height. Saravanakumar and Kumar [18] studied the effect of the attachment of baffles to the heat sink. They concluded that using of baffles increases the heat transfer.

The studies of heat sink performance do not limit to plate-fin and pin-fin heat sinks. Different geometries and types of fins have been investigated. This mainly includes laterally perforated-finned [19], radial heat sink with a perforated ring [20], honeycomb heat sink [21], and perforated rectangular fins [22–24].

The present work investigates numerically the effect of adding rods through the plate-fin heat sink. This configuration is found in some applications at which rods are used to support fins as shown in Fig. 1, and it can be used as an enhancement method of heat transfer. According to the best knowledge of the authors, this topic has not been studied in any previous works. Four configurations, with different numbers of rods starting from zero to six rods, have been studied. The shear-stress transport (SST) K–ω model has been selected to carry out this study. Two flow directions have been represented. Those two directions are used widely in many applications of plate-fin heat sinks, whereas some applications using suction flow and others depend on impinging flow.

2 Problem Description

Using rods through the fins can be applied in many applications, especially in electronic devices or to support fins in some air conditioning systems that depend on electronic devices for cooling or heating, as shown in Fig. 1. Four configurations have been suggested to investigate the improvement due to the presence of the rods through fins. The first configuration, as shown in Fig. 2, is the baseline case (plate fins without rods). The baseline case is like that was represented in Ref. [2] for validation. The base area of the heat sink is 40 mm × 39.7 mm with 5 mm thickness. Ten fins are attached to the base with 1 mm thickness, 3.3 mm space between fins, and 20 mm height above the base. Cases-1 to 3 have through-fin rods with 3 mm diameter with different numbers, as shown in Fig. 3(*a*), i.e., case-1 has two rods, case-2 has four rods, and case-3 has six rods. Figure 3(*b*) shows the positions of rods through the fins in the studied cases. Two directions of air flow are studied (impinging flow and suction flow) as shown in Fig. 4.

3 Numerical Simulation

3.1 Mesh Generation. The fluid domain has been created to investigate the required study by using one inlet with two outlets for impinging flow cases and two inlets with one outlet for suction flow cases as shown in Fig. 4. ANSYS FLUENT 17.2 has been used to construct geometry and mesh as well as to discretize and solve the governing equations. A grid independency test has been carried out. Table 1 represents numerical results for the base temperature and thermal resistance with different mesh configurations. The mesh size was ranged from 116,479 elements to 2,657,672 elements for the baseline case. The selected size is 752,039 to carry out the study. As the rods are added, the mesh size increases to 1,809,260 elements with case-3.

3.2 Boundary Conditions. The boundary conditions are considered similar to the experimental work of Kim et al. [2]. The air flow at inlet has four values of mass flowrate (0.000981, 0.001962, 0.002944, and 0.003925 kg/s) at 25 °C. The corresponding Reynolds numbers based on the inlet condition and the inlet hydraulic diameter (for impinging flow direction) are represented in Table 2. The Reynolds number can be calculated by using Eq. (1). For suction flow cases, the mass flowrate is divided equally on the two inlets to get the same flowrate and the Reynolds number is calculated at the outlet hydraulic diameter. The air properties, according to Kim et al. [2], are taken as density $(\rho_a) = 1.1774$ kg/m^3, dynamic viscosity $(\mu_a) = 1.8462 \times 10^{-5}$ kg/m s, specific heat $(c_{pa}) = 1.0057 \times 10^3$ J/kg K, and thermal conductivity $(k_a) = 0.02624$ W/m K. The heat sink is made of aluminum alloy 6061 with thermal conductivity $(k_s) = 171$ W/m K. The base of the heat sink subjected to a constant heat flux of 18,750 W/m^2. The outside walls of the heat sink as well as the duct walls are assumed adiabatic walls

$$\mathrm{Re}_{Dh} = \frac{4\dot{m}_a}{\pi \mu D_h} \tag{1}$$

3.3 Numerical Modeling. Different turbulent models have been tested to select the suitable one for the numerical analysis. As shown in Table 3, the SST K–ω model represents the smallest error. This agrees well with the fact that the K–ω SST model is commonly used for forced convection conditions in heat sinks [25]. So, the SST K–ω model is used to solve the momentum equations through this study considering the following assumptions:

- The air flow is three-dimensional, steady, and incompressible flow.
- Fluid–solid conjugate heat transfer.
- Radiative heat transfer from the heat sink is neglected.

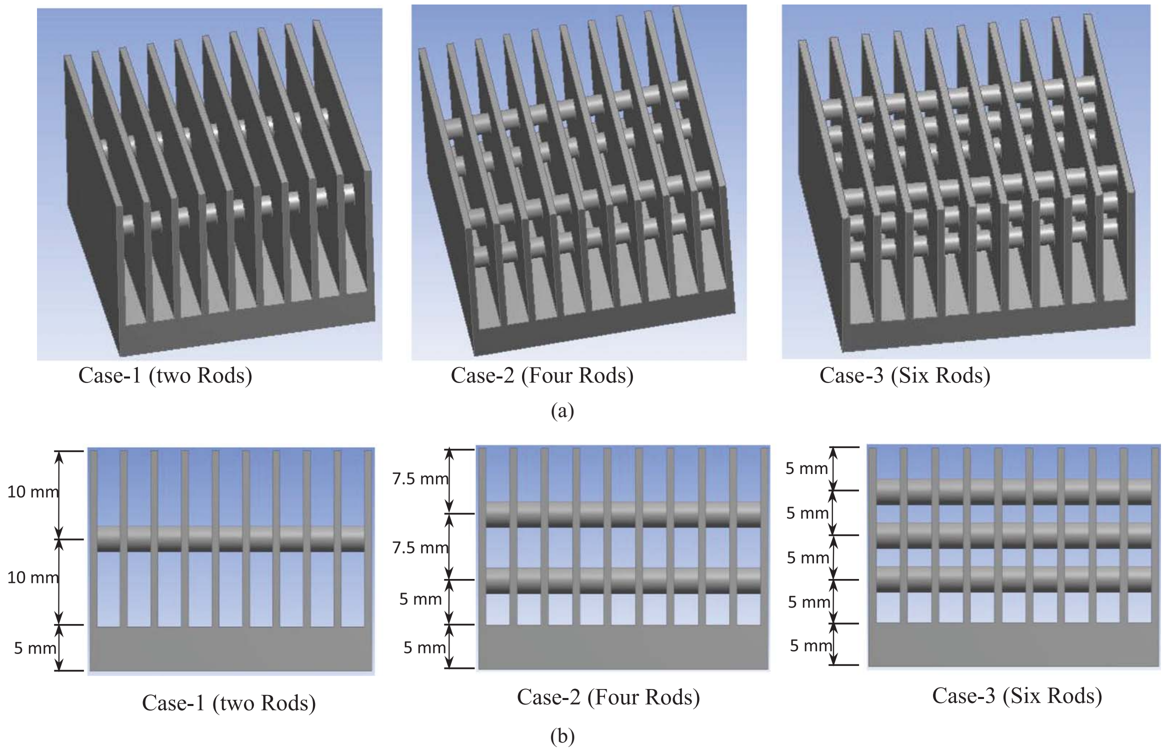

Fig. 3 Studied cases of rod through fins heat sink: (*a*) different configurations of rod through fins heat sink and (*b*) positions of the rods through fins in each case

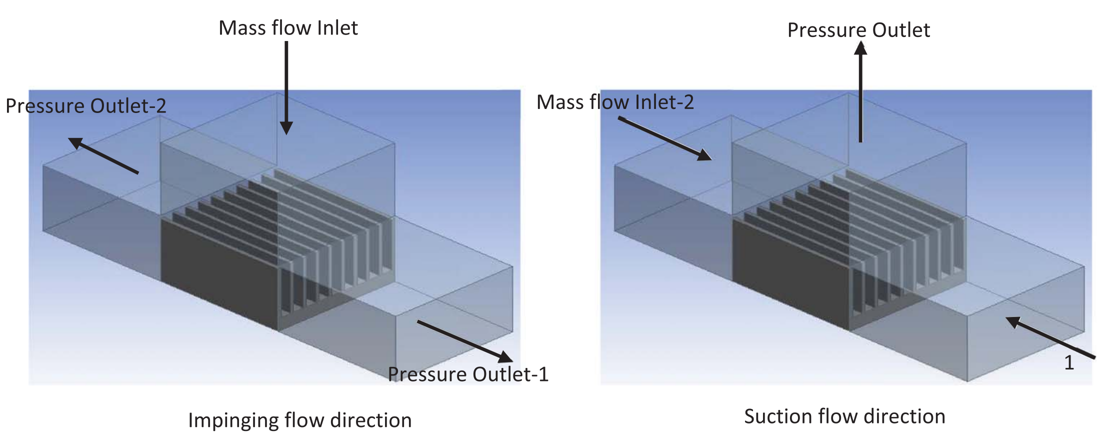

Fig. 4 Studied directions of the air flow with boundary conditions

The used governing equations are as follows:

The continuity equation is given by

$$\nabla(\rho\vec{U}) = 0 \tag{2}$$

The *N–S* equations across the x, y, and z directions are given by

$$\begin{aligned}
\nabla(\rho\vec{U}u) &= -\frac{\partial p}{\partial x} + \frac{\partial \tau_{xx}}{\partial x} + \frac{\partial \tau_{yx}}{\partial y} + \frac{\partial \tau_{zx}}{\partial z} \\
\nabla(\rho\vec{U}v) &= -\frac{\partial p}{\partial y} + \frac{\partial \tau_{xy}}{\partial x} + \frac{\partial \tau_{yy}}{\partial y} + \frac{\partial \tau_{zy}}{\partial z} \\
\nabla(\rho\vec{U}w) &= -\frac{\partial p}{\partial z} + \frac{\partial \tau_{xz}}{\partial x} + \frac{\partial \tau_{yz}}{\partial y} + \frac{\partial \tau_{zz}}{\partial z}
\end{aligned} \tag{3}$$

where ρ is the density of fluid, (u, v, and w) are velocity components in three directions, $\vec{U}$ is the velocity, τ is the viscous stress tensor, and p is the pressure.

The energy equation is given by

$$\nabla(\rho h\vec{U}) = -p\nabla\vec{U} + \nabla(k\nabla T) \tag{4}$$

where h is the aggregate enthalpy, k is the thermal conductivity, and T is the temperature.

The transport equations for the SST K–ω are given by

$$\frac{\partial}{\partial t}(\rho k) + \frac{\partial}{\partial x_i}(\rho k u_i) = \frac{\partial}{\partial x_j}\left(\Gamma_k \frac{\partial k}{\partial x_j}\right) + G_k - Y_k + S_k \tag{5}$$

$$\frac{\partial}{\partial t}(\rho\omega) + \frac{\partial}{\partial x_i}(\rho\omega u_i) = \frac{\partial}{\partial x_j}\left(\Gamma_\omega \frac{\partial \omega}{\partial x_j}\right) + G_\omega - Y_\omega + D_\omega + S_\omega \tag{6}$$

where G_k represents the generation of turbulence kinetic energy due to mean velocity gradients and G_ω represents the generation of ω

Table 1 Results of the grid independency study

Mesh	No. of elements	Base temperature (°C)	R_{th}	Difference in temp. with previous (%)	Difference in R_{th} with previous (%)
Mesh1	116,479	65.715	1.457	–	–
Mesh2	221,571	65.361	1.300	0.10	10.77
Mesh3	752,039	65.031	1.271	0.10	2.19
Mesh4	2,657,672	65.402	1.271	−0.01	0.03

Table 2 Studied range of mass flowrate and corresponding Reynolds number

No.	Mass flowrate (kg/s)	Corresponding Re
1	0.000981	1333.63
2	0.001962	2667.26
3	0.002944	4000.89
4	0.003925	5334.52

Table 3 Tested turbulent models (Re = 5334)

Model	Thermal resistance R_{th}	Error (%)
Experiment	1.26	—
k–ε-standard	1.40	11.22
k–ε-RNG	1.43	13.23
k–ε-Realizable	1.44	14.32
k–ω-BSL	1.29	2.22
k–ω-SST	1.27	0.92

and they calculated as follows:

$$G_k = -\rho \overline{u_i' u_j'} \frac{\partial u_j}{\partial x_i} \tag{7}$$

$$G_\omega = \alpha \frac{\omega}{k} G_k \tag{8}$$

And, Γ_k and Γ_ω represent the effective diffusivity of k and ω, respectively. Y_k and Y_ω represent the dissipation of k and ω due to turbulence. D_ω represents the cross-diffusion term. S_k and S_ω are user-defined source terms.

4 Calculation Procedure

The thermal resistance, R_{th}, is used to compare the present work with the previous experimental work and to estimate the enhancement of the performance of the plate heat sink. Equation (9) is used to calculate the thermal resistance

$$R_{th} = \frac{1}{\bar{h} A_T} \tag{9}$$

where $\bar{h}$ is the mean heat transfer coefficient and A_T is the total area of the heat sink subjected to the fluid flow.

The mean heat transfer coefficient can be calculated by using Eq. (10) and the total area by using Eq. (11)

$$\bar{h} = \frac{Q}{A_T (T_b - T_{avr})} \tag{10}$$

$$A_T = WL + 2H(L(N_f - 1) + tN_f) + 2BW + N_R \pi D_R (W - N_f t) \tag{11}$$

where Q is the heat transfer rate given by Eq. (12), T_b is the fin base temperature and T_{avr} is the average air temperature given by Eq. (13). W and L are the width and length of the heat sink, respectively, N_f, H, and t are the fins number, height above the base, and thickness, respectively. While B is the base height, N_R and D_R are the rods through fin number and diameter, respectively

$$Q = \dot{m}_a C_{pa} (T_{out} - T_{in}) \tag{12}$$

$$T_{avr} = \frac{(T_{out} - T_{in})}{2} \tag{13}$$

where $\dot{m}_a$ and C_{pa} are the mass flowrate (kg/s) and specific heat of air at the average temperature T_{avr}, respectively. T_{out} and T_{in} are the outlet and inlet temperature of air, respectively. The performance of the heat sink can be also represented and analyzed by calculating the Nusselt number by using Eq. (14)

$$\overline{\mathrm{Nu}} = \frac{\bar{h} D_h}{K_a} \tag{14}$$

where D_h is the hydraulic diameter of the inlet of impinging flow direction cases and of the outlet of the suction flow direction cases. K_a is the thermal conductivity of the air based on the average temperature of air. The pressure drop, Δp, is an important parameter to estimate the effect of using through fins rods on the pumping power. Equations (15) and (16) are used to calculate the pressure drop and the pumping power, respectively

$$\Delta P = P_{out} - P_{in} \tag{15}$$

$$P_P = \frac{\Delta P \, \dot{m}_a}{\rho_a} \tag{16}$$

5 Results and Discussion

5.1 Validation of the Model. For the validation of the numerical model, a comparison with the previous experimental work of Kim et al. [2] was carried out. The comparison is represented for impingement flow at different mass flowrate with the baseline case. Figures 5 and 6 represent the thermal resistance and pressure drop of air at different mass flowrate, respectively. Figure 5 shows a good agreement between the numerical and experimental results with maximum discrepancy of about 2.8%. A good agreement is also obtained with the pressure drop with about 10% discrepancy. An acceptable explanation for the difference may be due to thermal losses and measurement errors [3]. Therefore, it can be concluded that the used numerical model is accurate enough to carry out the investigation of using rods through the plate-fin heat sink.

5.2 Effectiveness of the Heat Sink. The effectiveness term is used to explain the degree of achievement of the heat sink surface temperature reduction. It is also used to unify of the measured range to be easy in comparison. Equation (17) is used to calculate the effectiveness of the heat sink surface. If the value of the effectiveness close to zero, that means the heat sink temperature is high and the cooling is not effective. As the effectiveness increases, the cooling becomes more effective

$$\varepsilon = \frac{T_b - T_s}{T_b - T_{in}} \tag{17}$$

Figures 7 and 8 show the detailed effectiveness of the heat sink at mass flowrates of 0.00981 (Re = 1334) and 0.003925 (Re = 5334) for the studied cases with impinging and suction flow directions, respectively. As expected, Figs. 7 and 8 show that higher effectiveness is achieved as the number of rods increases (the surface area increases), causing lower surface temperature of the heat sink. Therefore, the heat sink surface temperature is reduced, as the number of rods increases. The figures show also that the higher

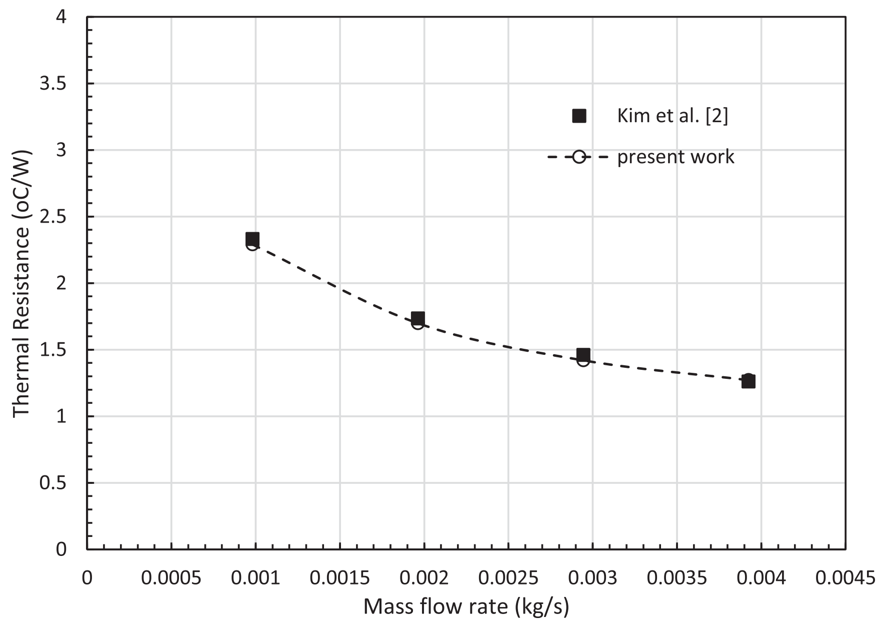

Fig. 5 Validation of the present work for thermal resistance with baseline case, impingement flow direction

Reynolds number, the more effectiveness achieved. To determine the optimum case and flow directions, thermal resistance, pressure drop, and Nusselt number should be represented and compared. The optimum case is assumed that the case which has the lowest thermal resistance with relatively low pumping power and high Nusselt number. Section 5.3 represents the thermal resistance and pumping power for the studied cases.

5.3 Thermal Resistance and Pumping Power. In this section, the effects of the using rods through fins with impinging and suction flows on the thermal resistance and pumping power are represented and discussed. Figure 9 shows the effect of using different numbers of rods on the thermal resistance of the heat sink. The figure shows that as the Reynolds number increases, the thermal resistance decreases for all studied cases and the studied directions of flow. The thermal resistance with impinging flow direction is less than that of suction flow direction for all studied range of the Reynolds number and all studied cases. In suction flow cases, using rods through fins reduces the thermal resistance by significant values. At $Re = 1334$, the thermal resistance reduces by 5.16% with case-1, 2.8% with case-2, and 6.9% with case-3 as compared by the baseline case for suction flow direction. While for impinging flow direction, it reduces by 0.68% with case-1, 5.28% with case-2, and 5.27% with case-3. At $Re = 5334$, the thermal resistance reduces by 19.2% with case-1, 24% with case-2, and 31.8% with case-3 for suction flow direction, while it reduces by 3% with case-1, 13.4% with case-2, and 15.3% with case-3 for impinging flow direction. It is clear from the above analysis that although the impinging flow direction represents lower thermal resistance, the using of rod

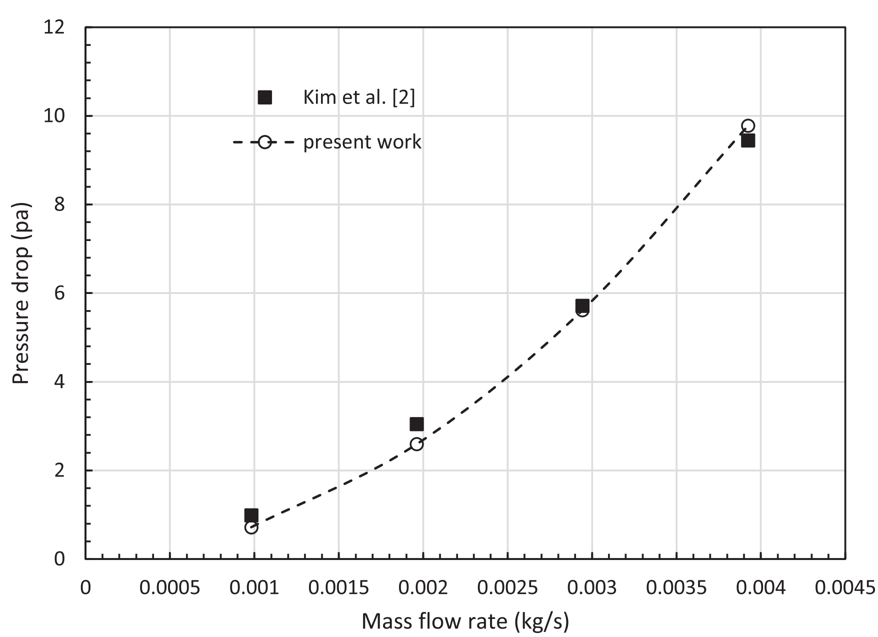

Fig. 6 Validation of the present work for pressure drop with baseline case, impingement flow direction

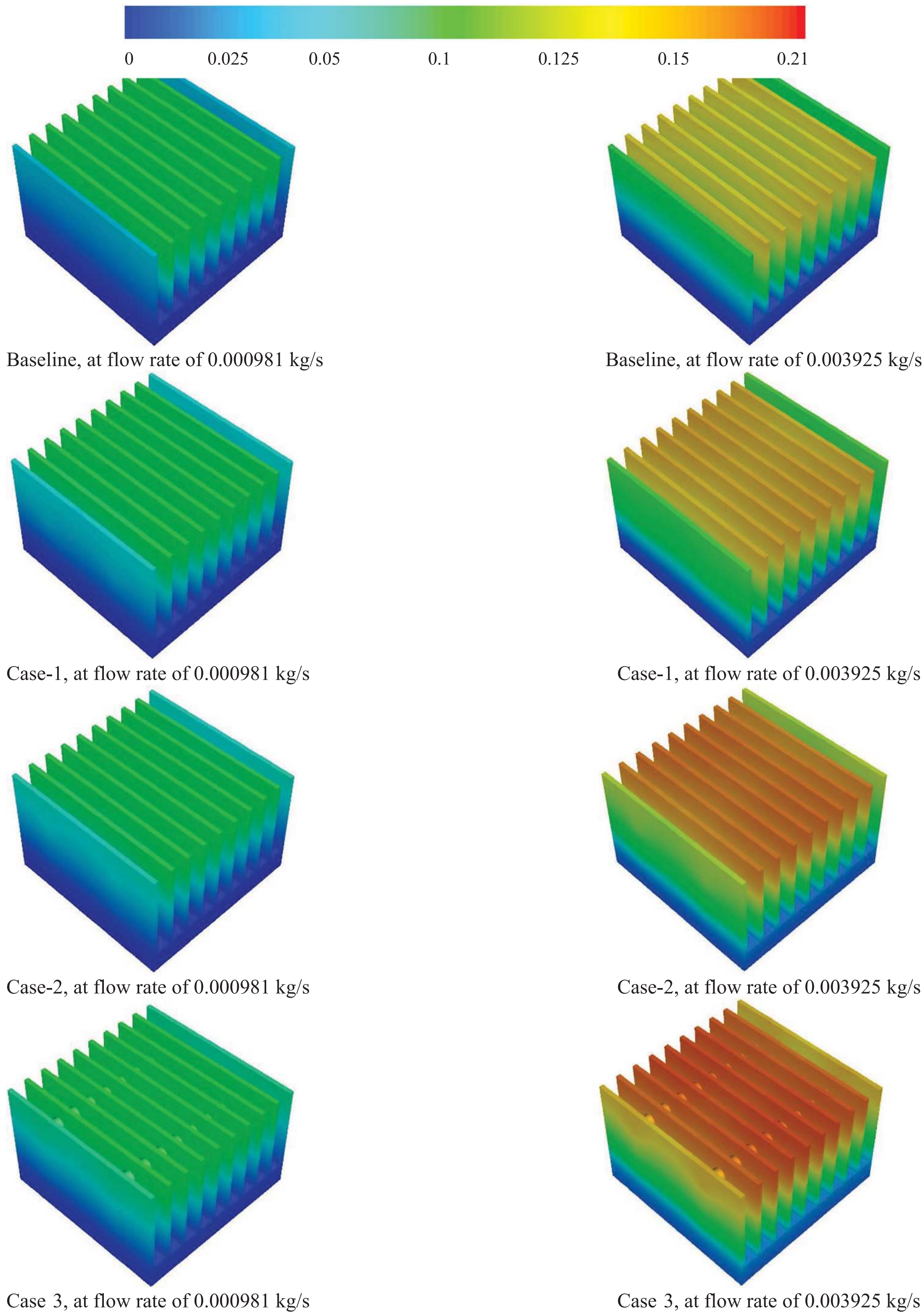

Fig. 7 The detailed heat sink effectiveness for studied cases with impinging flow direction

through fins represents higher effect in case of suction flow. The presence of the rods increases the contact surface area; however, it increases also the turbulence of the flow through the heat sink fins as shown in Fig. 10. Figure 10 shows the velocity contours colored by vorticity magnitude for studied cases at Re = 5334. The figure represents *x*–*y* plan at the middle distance between fins. The figure shows that higher vorticities appear around rods, causing better heat transfer between fin surfaces and air flow. In case of suction flow, the presence of rods increases the amount of the fluid that in contact with the heat sink base surface and the turbulence near the base. On the contrary, in case of impinging flow direction, the presence of the rods may block part of the flow impinging the base surface but in the same time increases the flow turbulent and thus the heat transfer from the fins.

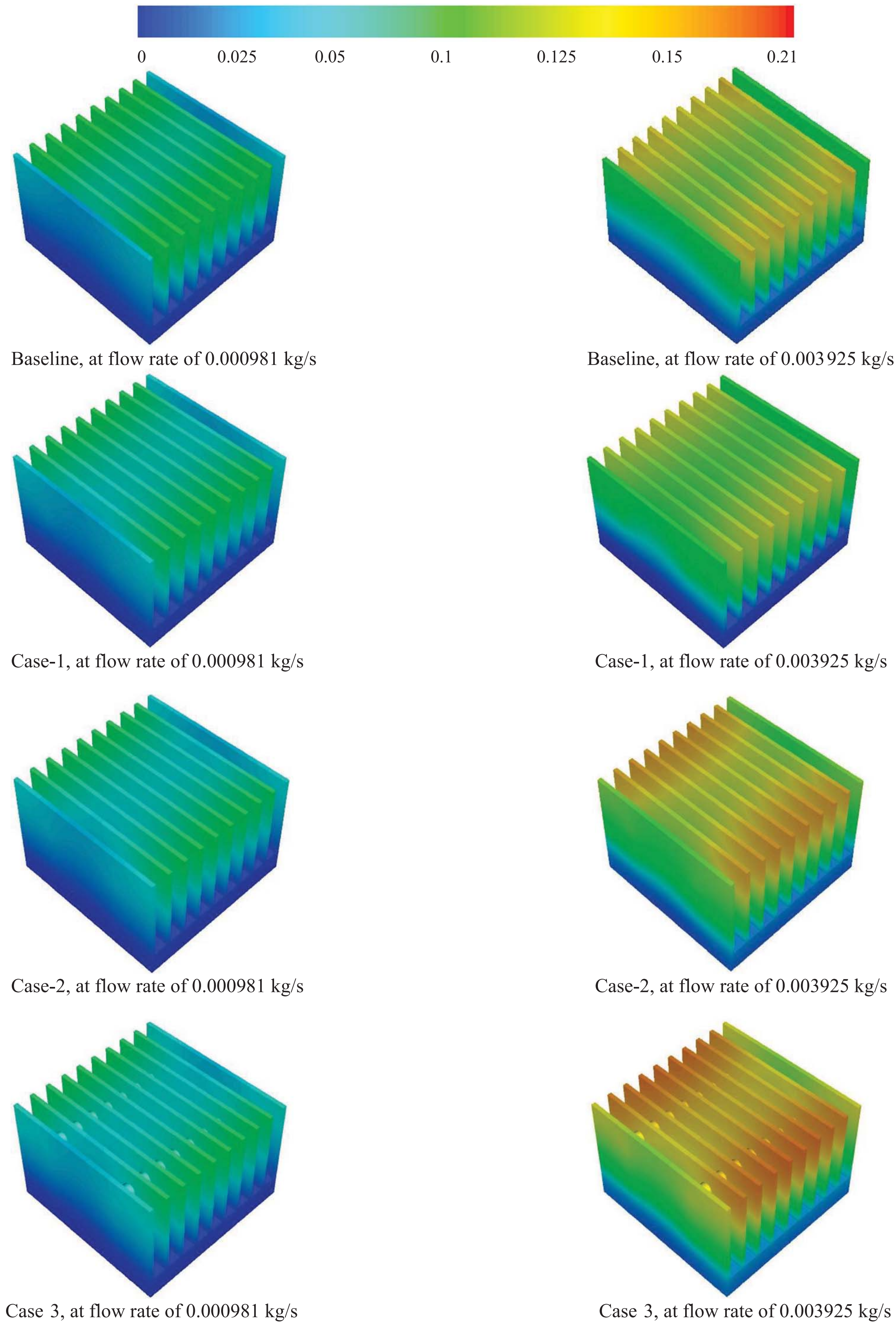

Fig. 8 The detailed heat sink effectiveness for studied cases with suction flow direction

To represent a complete understanding of the effect of adding rods through fins, the pumping power should be represented. Figure 11 shows the pressure drop through the heat sink for studied cases at different Reynolds numbers for suction and impinging flow directions. At low Reynolds number, the use of rods has no significant effect of pressure drop. As the Reynolds number increases, the pressure drop increases and the effect of using rods becomes more significant. The pressure drop for impinging flow direction is less than that for suction flow direction for all studied cases on the studied range of the Reynolds number. As the

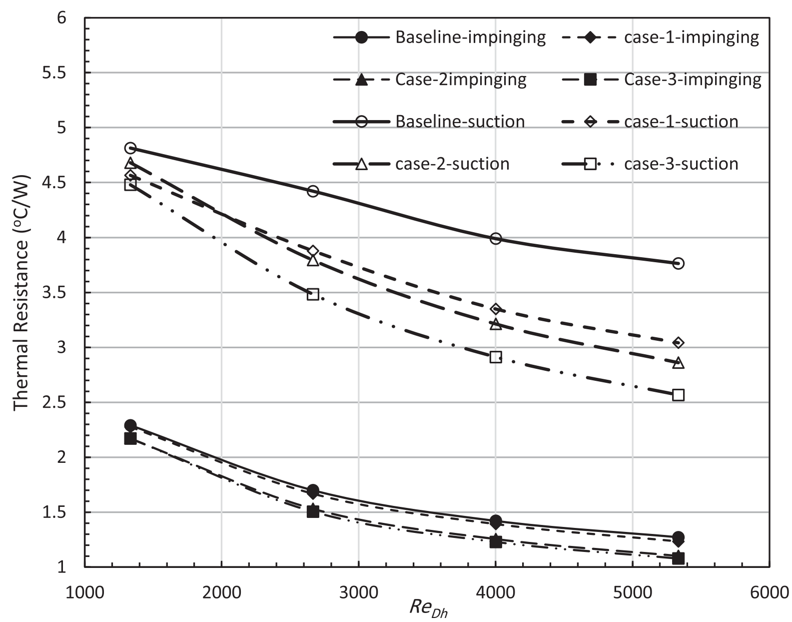

Fig. 9 The thermal resistance of the heat sink for impinging and suction flow directions at different Re with the studied cases

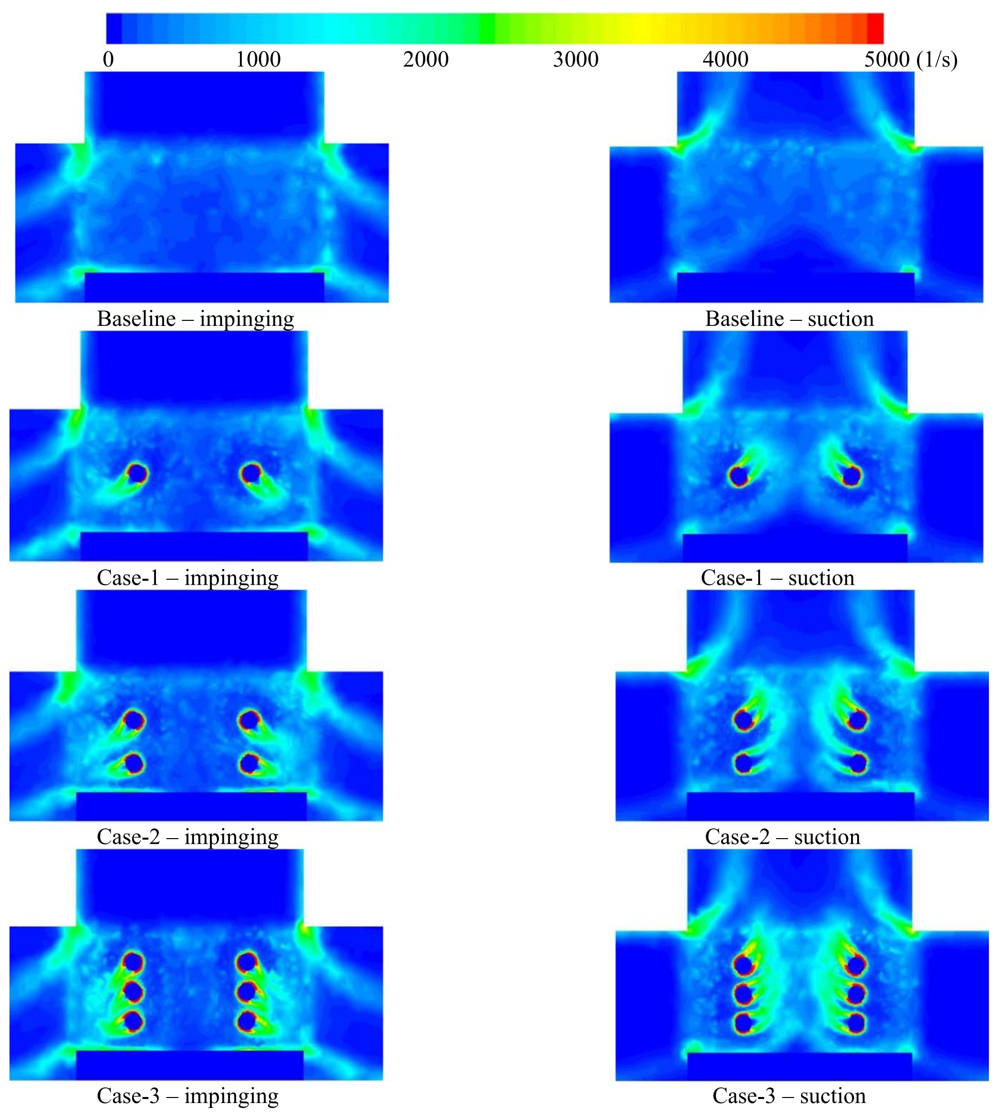

Fig. 10 Velocity contours colored by vorticity magnitude for studied cases at Re = 5334

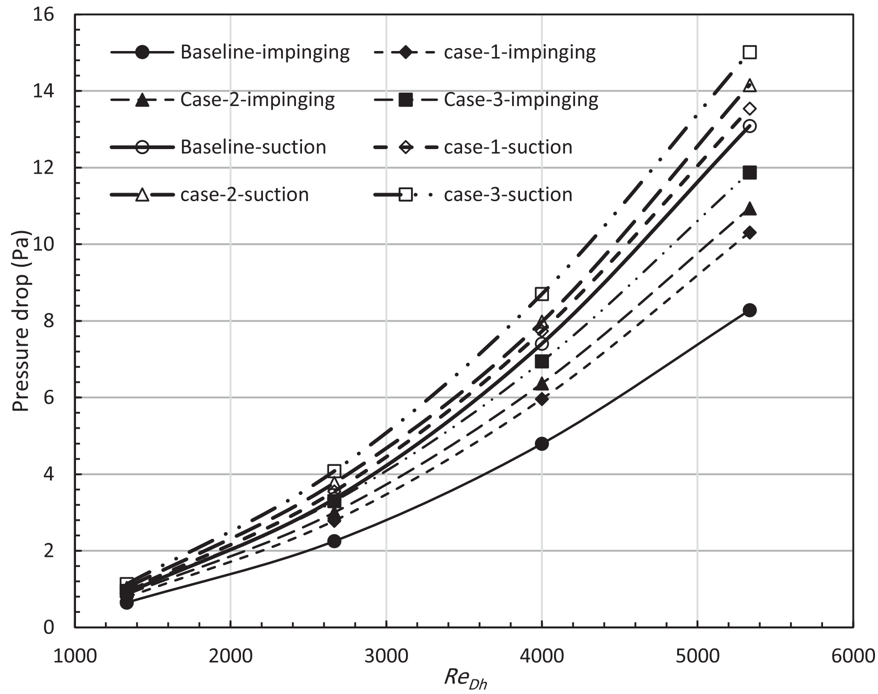

Fig. 11 The pressure drop through the heat sink for impinging and suction flow directions at different Re with the studied cases

number of rods increases, the pressure drop increases. The percentage increase in pressure drop with case-3 as compared with the baseline case is 43.5% for Re = 5334 with impinging flow direction against 14.7% with suction flow direction. As the turbulent increases due to the use of rods, the pressure drop increases. Suction flow direction has more pressure drop and required more pumping power to overcome the friction resistance than that required by impinging flow direction. The thermal resistance versus pumping power has been represented in Fig. 12. The figure shows that impinging flow direction is more effective than suction flow direction. The required pumping power for case-2 and case-3 are close to each other to get the same thermal resistance. So, case-2 is the suitable one to get less thermal resistance with low pumping power as compared with other cases because it has less area and material of construction than case-3. To represent the heat transfer performance of the heat sink for the studied cases, Fig. 13 is used to show the effect of using rods and flow directions on the Nusselt number. In case of suction flow direction, the

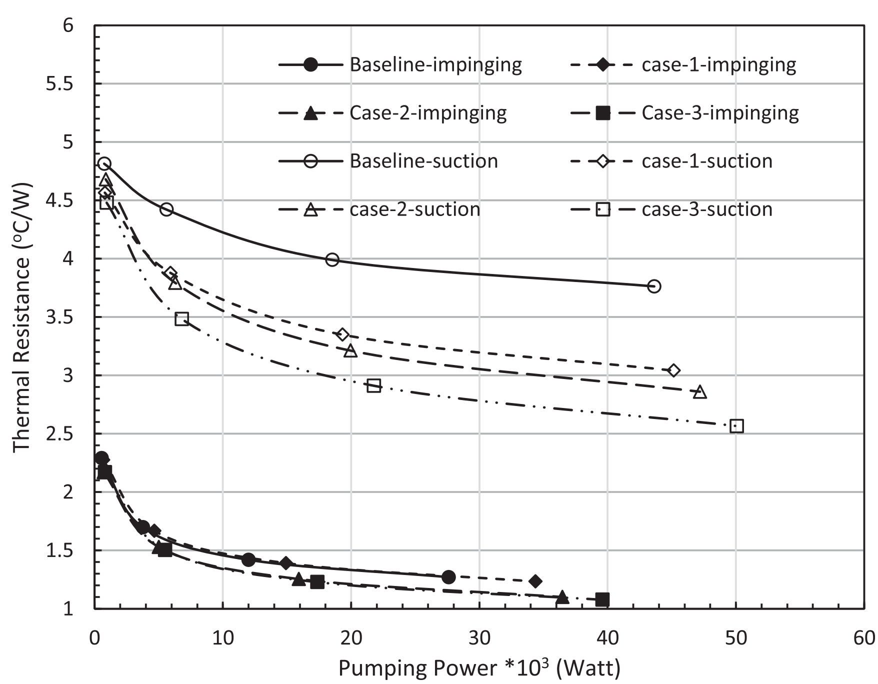

Fig. 12 The thermal resistance versus pumping power of the heat sink for impinging and suction flow directions

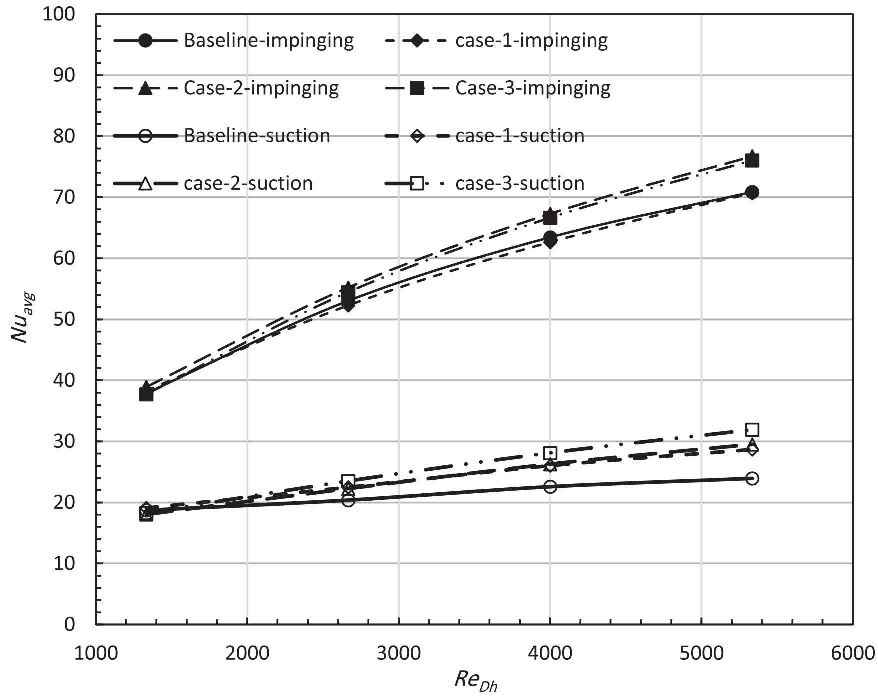

Fig. 13 Nusselt number of the heat sink for impinging and suction flow directions

maximum range of increasing in the Nusselt number is 13.6, while it is 38.3 in case of impinging flow direction. That gives an idea how the using of rods has more effect on heat transfer with the impinging flow direction. Case-2, with impinging flow direction, represents the highest Nusselt number for all studied values of the Reynolds number.

6 Conclusion

Using rods through fins is a new configuration to improve the performance of the plate-fin heat sink. In this research, the effect of using rods through fins has been investigated numerically. According to the most knowledge of the authors, this configuration has not been studied in previous works. Two different flow directions have been investigated (impinging and suction flow directions). Four cases, with different numbers of rods through fins, have been studied. The results show that

(1) The impinging flow direction represents higher cooling of the heat sink than that of suction flow direction.
(2) As the Reynolds number increases, the thermal resistance decreases, causing more cooling while the pressure drop increases.
(3) As the number of rods increases, the thermal resistance decreases, while the required pumping power increases in both impinging and suction flow directions.
(4) The presence of the rods increases the turbulent of the flow causing more heat removal from the heat sink surface. But on the other hand, it increases the friction through the fins causing higher required pumping power.
(5) At low Reynolds number, the use of rods through the fins has no significant effect on the thermal resistance and pumping power of the heat sink.
(6) The heat sink with four rods (case-2) shows the highest Nusselt number for impinging flow direction.
(7) The heat sink with six rods (case-3) and the heat sink with four rods (case-2) are close to each other in their performance.
(8) Case-2 represents the optimum design to get lower thermal resistance and higher Nusselt number at accepted range of pumping power.

Acknowledgment

The authors extend their appreciation to the Deanship of Scientific Research at King Khalid University for funding this work through Research Group Project under grant number (R.G.P1./95/40).

Nomenclature

t = fin thickness (m)
B = base height (m)
H = height of the heat sink, above the base (m)
K = thermal conductivity (W/m K)
L = length of the heat sink (m)
T = temperature (K)
W = width of the heat sink (m)
A_T = total surface area of the heat sink
D_R = rod diameter (m)
D_h = hydraulic diameter (m)
N_f = number of fins
N_R = number of rods
P_P = pumping power (W)
$\bar{h}$ = mean heat transfer coefficient
$\dot{m}$ = mass flowrate (kg/s)
Nu = Nusselt number
Re = Reynolds number
Δp = pressure drop (Pa)

Greek Symbols

μ = dynamic viscosity of the air (Pa · s)
ρ = air density (kg/m^3)

Subscripts

a = air
b = base

s = heat sink surface
Dh = at hydraulic diameter
in = air inlet
avr = average
out = air outlet

Superscripts

$^{-}$ = averaged

References

[1] Khattak, Z., and Ali, H. M., 2019, "Air Cooled Heat Sink Geometries Subjected to Forced Flow: A Critical Review," Int. J. Heat Mass Transfer, **130**, pp. 141–161.
[2] Kim, D. K., Kim, S. J., and Bae, J. K., 2009, "Comparison of Thermal Performances of Plate-Fin and Pin-Fin Heat Sinks Subject to an Impinging Flow," Int. J. Heat Mass Transfer, **52**(15–16), pp. 3510–3517.
[3] Biber, C. R., 1997, "Pressure Drop and Heat Transfer in an Isothermal Channel With Impinging Flow," IEEE Trans. Compon. Packag. Manuf. Technol. A, **20**, pp. 458–462.
[4] Kondo, Y., Behnia, M., Nakayama, W., and Matsushima, H., 1998, "Optimization of Finned Heat Sinks for Impingement Cooling of Electronic Packages," J. Electron. Packag., **120**(3), pp. 259–266.
[5] Duan, Z., and Muzychka, Y. S., 2006, "Experimental Investigation of Heat Transfer in Impingement Air Cooled Plate Fin Heat Sinks," J. Electron. Packag., **128**(4), pp. 412–418.
[6] Sathe, S., Kelkar, K. M., Karki, K. C., Tai, C., Lamb, C., and Patankar, S. V., 1997, "Numerical Prediction of Flow and Heat Transfer in an Impingement Heat Sink," J. Electron. Packag., **119**(1), pp. 58–63.
[7] Ledezma, G., Morega, A. M., and Bejan, A., 1996, "Optimal Spacing Between Pin Fins With Impinging Flow," ASME J. Heat Transfer, **118**(3), pp. 570–577.
[8] Kondo, Y., Matsushima, H., and Komatsu, T., 2000, "Optimization of Pin Fin Heat Sinks for Impingement Cooling of Electronic Packages," J. Electron. Packag., **122**(3), pp. 240–246.
[9] Issa, J. S., and Ortega, A., 2006, "Experimental Measurements of the Flow and Heat Transfer of a Square Jet Impinging on an Array of Square Pin Fins," J. Electron. Packag., **128**(1), pp. 61–70.
[10] Choudhary, V., Kumar, M., and Patil, A. K., 2019, "Experimental Investigation of Enhanced Performance of Pin Fin Heat Sink With Wings," Appl. Therm. Eng., **155**, pp. 546–562.
[11] Bar-Cohen, A., 1996, "Thermal Management of Electric Components With Dielectric Liquids," Proceedings of ASME/JSME Thermal Engineering Joint Conference, Maui, HI, J. R. Lloyd and Y. Kurosaki, eds., vol. 2, pp. 15–39.
[12] Kondo, Y., Matsushima, H., and Ohashi, S., 1999, "Optimization of Heat Sink Geometries for Impingement Air-Cooling of LSI Packages," Heat Transfer Asian Res., **28**, pp. 138–151.
[13] Li, H.-Y., Chao, S.-M., and Tsai, G.-L., 2005, "Thermal Performance Measurement of Heat Sinks With Confined Jet by Infrared Thermography," Int. J. Heat Mass Transfer, **48**(25–26), pp. 5386–5394.
[14] Kim, S. J., Kim, D.-K., and Oh, H. H., 2008, "Comparison of Fluid Flow and Thermal Characteristics of Plate-Fin and Pin-Fin Heat Sinks Subject to a Parallel Flow," Heat Transfer Eng., **29**(2), pp. 169–177.
[15] Wong, K. C., and Indran, S., 2013, "Impingement Heat Transfer of a Plate Fin Heat Sink With Fillet Profile," Int. J. Heat Mass Transfer, **65**, pp. 1–9.
[16] Hussain, A. A., Freegah, B., Khalaf, B. S., and Towsyfyan, H., 2019, "Numerical Investigation of Heat Transfer Enhancement in Plate-Fin Heat Sinks: Effect of Flow Direction and Fillet Profile," Case Stud. Therm. Eng., **13**, p. 100388.
[17] Jeon, D., and Byon, C., 2017, "Thermal Performance of Plate Fin Heat Sinks With Dual-Height Fins Subject to Natural Convection," Int. J. Heat Mass Transfer, **113**, pp. 1086–1092.
[18] Saravanakumar, T., and Kumar, D. S., 2019, "Performance Analysis on Heat Transfer Characteristics of Heat SINK With Baffles Attachment," Int. J. Therm. Sci., **142**, pp. 14–19.
[19] Shaeri, M. R., and Bonner, R., 2017, "Heat Transfer and Pressure Drop in Laterally Perforated-Finned Heat Sinks Across Different Flow Regimes," Int. Commun. Heat Mass Transfer, **87**, pp. 220–227.
[20] Li, B., Jeon, S., and Byon, C., 2016, "Investigation of Natural Convection Heat Transfer Around a Radial Heat Sink With a Perforated Ring," Int. J. Heat Mass Transfer, **97**, pp. 705–711.
[21] Ozsipahia, M., Subasia, A., Gunesa, H., and Sahin, B., 2018, "Numerical Investigation of Hydraulic and Thermal Performance of a Honeycomb Heat Sink," Int. J. Therm. Sci., **134**, pp. 500–506.
[22] Awasarmol, U. V., and Pise, A. T., 2015, "An Experimental Investigation of Natural Convection Heat Transfer Enhancement From Perforated Rectangular Fins Array at Different Inclinations," Exp. Therm. Fluid. Sci., **68**, pp. 145–154.
[23] Alessa, A. H., Maqableh, A. M., and Ammourah, S., 2009, "Enhancement of Natural Convection Heat Transfer From a Fin by Rectangular Perforations With Aspect Ratio of Two," Int. J. Phys. Sci., **4**, pp. 540–547.
[24] Huang, G. J., Wong, S. C., and Lin, C. P., 2014, "Enhancement of Natural Convection Heat Transfer From Horizontal Rectangular Fin Arrays With Perforations in Fin Base," Int. J. Therm. Sci., **84**, pp. 164–174.
[25] Yoon, Y., Park, S. J., Kim, D. R., and Lee, K.-S., 2018, "Thermal Performance Improvement Based on the Partial Heating Position of a Heat Sink," Int. J. Heat Mass Transfer, **124**, pp. 752–760.